Science
AAAS

Structural basis of membrane disruption and cellular toxicity by α-synuclein oligomers

Giuliana Fusco[1,2], Serene W. Chen[1,2], Philip T. F. Williamson[3], Roberta Cascella[4], Michele Perni[1], James A. Jarvis[2], Cristina Cecchi[4], Michele Vendruscolo[1], Fabrizio Chiti[4], Nunilo Cremades[5], Liming Ying[6], Christopher M. Dobson[1,*] and Alfonso De Simone[2,*]

[1]*Department of Chemistry, University of Cambridge, Cambridge CB2 1EW, UK*
[2]*Department of Life Sciences, Imperial College London, London SW7 2AZ, UK*
[3]*Centre for Biological Sciences/Institute for Life Sciences, University of Southampton, Southampton SO17 1BJ, UK.*
[4]*Department of Experimental and Clinical Biomedical Sciences, Section of Biochemistry, University of Florence, 50134 Florence, Italy.*
[5]*Biocomputation and Complex Systems Physics Institute (BIFI)-Joint Unit BIFI-IQFR (CSIC), University of Zaragoza, 50018 Zaragoza, Spain.*
[6]*Molecular Medicine, National Heart and Lung Institute, Imperial College London, London SW7 2AZ, UK*

*Correspondence to: cmd44@cam.ac.uk or adesimon@imperial.ac.uk

One Sentence Summary: Oligomers of α-synuclein generate neuronal damage when insertion of a highly structured core causes disruption of membrane integrity.

Abstract: Oligomeric species populated during the aggregation process of α-synuclein have been linked to neuronal impairment in Parkinson's disease and related neurodegenerative disorders. By using solution and solid-state NMR techniques in conjunction with other structural methods, we identified the fundamental characteristics that enable toxic α-synuclein oligomers to perturb biological membranes and disrupt cellular function; these include a highly lipophilic element that promotes strong membrane interactions and a structured region that inserts into lipid bilayers and disrupts their integrity. In support of these conclusions, mutations that target the region that promotes strong membrane interactions by α-synuclein oligomers suppressed their toxicity in neuroblastoma cells and in primary cortical neurons.

The aggregation of α-synuclein (αS) into amyloid fibrils within Lewy bodies is associated with Parkinson's disease (PD) and a range of other debilitating neurodegenerative disorders (*1-9*). The primary pathogenic agents in these conditions are thought to be the oligomeric species populated in the self-assembly of αS, particularly through their aberrant interactions with biological membranes (*10-16*). Here we investigated two types of stabilized αS oligomers with significantly different toxicities (*17, 18*), which we designated as *type-A** and *type-B**. Their Förster resonance energy transfer (FRET) signatures (Fig. 1A), as well as other structural and biological properties (Fig. 1), closely matched those of the previously identified transient forms of non-toxic (type A) and toxic (type B) αS oligomers (*19*).

The two oligomeric forms of αS had similar sizes and morphologies (Fig. 1B-C), yet exhibited very different abilities to disrupt lipid bilayers. When incubated in vitro with small unilamellar vesicles (SUVs), *type-A** oligomers induced only a marginal release of encapsulated calcein molecules, comparable to that induced by αS monomers and mature fibrils (Fig. 1D). In contrast, *type-B** oligomers induced over ten times more calcein release, indicating that these oligomers generate considerable disruption of acidic lipid bilayers (Fig. 1D). We observed similar loss of membrane integrity in vivo upon incubation of *type-B** αS oligomers with human neuroblastoma SH-SY5Y cells and rat primary cortical neurons, and only marginal effects upon incubation with *type-A** oligomers, monomers and mature fibrils of αS (Fig. 1E, G).

The significant disruption of synthetic and cellular membranes by *type-B** αS oligomers, but not *type-A** species, was strongly correlated with their ability to generate cellular toxicity. Thus *type-B** αS oligomers, but not monomers, *type-A** oligomers and αS fibrils, induced substantial increases of intracellular reactive oxygen species (ROS, Fig. S1A) and reduced the mitochondrial activity in neuronal cells (MTT, Fig. 1F). The cellular damage that *type-B** αS oligomers induced in this manner reproduces a variety of patho-physiological effects observed in neuronal models of PD obtained by inducing pluripotent stem cell-derived neurons from a patient with triplication of the αS gene (*20-22*).

To probe the structural properties of the two types of αS oligomers, we used solid-state NMR (ssNMR) spectroscopy. Correlations between carbon atoms of residues located in rigid regions of the oligomers were detected using ^{13}C-^{13}C dipolar-assisted rotational resonance (DARR) correlation spectra, measured using magic angle spinning (MAS). ^{13}C-^{13}C-DARR spectra of *type-A** and *type-B** oligomers revealed fundamental differences in the structural nature of the two species (Fig. 2A), with a significant content of β-sheet identified in the rigid regions of the *type-B** oligomers and negligible secondary structure content associated with the rigid regions of *type-A** oligomers (Fig. 2A and S2). The assignment of the ^{13}C-^{13}C-DARR peaks was performed using an approach (*23-25*) that combines information from solution-state chemical exchange saturation transfer (*23, 26, 27*) (CEST, see Methods and Fig. S3) with known assignments of fibrillar (*5*) and monomeric (*25*) states of αS. This approach revealed that the resonances in the ^{13}C-^{13}C-DARR spectra of the two types of oligomers belong to specific regions spanning residues 3-36 and 70-88 in *type-A** and *type-B** species, respectively (Table S1).

Highly mobile regions of the two forms of αS oligomers were detected using INEPT measurements in MAS ssNMR (Fig. 2B). Both types of oligomers contained a large number of highly mobile residues (45 in *type-A** and 67 in *type-B**, Table S1), whose resonances overlapped with those in the ^{1}H-^{13}C-HSQC spectra of disordered monomeric αS in solution (Fig. S4). Although both oligomeric species possessed a flexible C-terminal region (43 and 40 highly

mobile C-terminal residues for *type-A** and *type-B**, respectively), the N-terminal region of αS was highly dynamic only in the *type-B** oligomers (0 and 26 highly mobile N-terminal residues for *type-A** and *type-B**, respectively). Furthermore, the mobile regions of the *type-A** αS oligomers also included residues from the NAC region (Fig 2B), a finding consistent with the low FRET efficiency observed for the *type-A** relative to the *type-B** oligomers when the fluorophores were attached to residue 90, itself located in the NAC region (Fig. 1A).

The ssNMR characterization of the two types of αS oligomers was supported by Fourier transform infrared (FT-IR) measurements (Fig. S5), showing signals characteristic of both random-coil and β-sheet structure in the case of the *type-B** αS oligomers, but indicating a predominantly unstructured conformation for the *type-A** species. Further indication of the association with the core of the oligomers in *type-A** and *type-B** species was provided by CEST experiments (Fig. S3). *Type-A** oligomers revealed extensive saturation in the 40 N-terminal residues of the protein, indicating a significant degree of association of this region with the core of the oligomers. For *type-B** oligomers, CEST experiments showed no saturation associated with either the N- or C- terminal regions of the protein or with residues of three of the four major hydrophobic segments of the αS sequence (residues 36-41, 47-56, 88-95), in contrast to the significant saturation observed for the hydrophobic segment 70-79. The identification of highly dynamic regions in the two types of αS oligomers was consistent with a dot blot analysis carried out using a primary antibody that bind the N-terminal region of αS. This indicated that the N-terminal region is more accessible in *type-B** than in *type-A** species (Fig. S6). In contrast, dot blot analysis carried out using a primary antibody targeting the C-terminal region of αS indicated that the C-terminus is accessible to a similar extent in both types of oligomers (Fig. S6).

We next probed the interaction of the two types of αS oligomers with SUVs composed of DOPE:DOPS:DOPC lipids in a ratio of 5:3:2 (see Methods), which are good mimics of synaptic vesicles for composition and physical properties (*24, 25*). Fluorescence correlation spectroscopy (FCS) in combination with confocal microscopy showed that both types of oligomers bind the SUVs with high affinity, with the *type-B** oligomers binding more strongly relative to the *type-A** species (Fig. 3A and S7). *Type-B** αS oligomers also colocalized with the plasma membrane of primary cortical neurons (Fig. 3B).

To characterize the levels of membrane insertion of the two types of αS oligomers, we carried out paramagnetic relaxation enhancement (PRE) experiments using MAS ssNMR, in which small quantities of lipid molecules labeled with a paramagnetic center (PC) were incorporated into the bilayers (*24, 25*). When the PC was located in the hydrophilic head groups of the lipid molecules (see Methods), selective quenching of a number of ^{13}C-^{13}C-DARR resonances was observed in the spectra of both types of αS oligomers (Fig. S8). This indicates in both cases strong interactions with the membrane surface. In contrast, when the PC was positioned within the interior of the lipid bilayer, enhanced relaxation of ^{13}C-^{13}C-DARR resonances was observed only for the *type-B** oligomers (Fig. 3C); this suggests that *type-B** oligomers can insert into the hydrophobic interior of the lipid bilayer while the *type-A** oligomers remain bound exclusively to the membrane surface (Fig. 3E-F). In addition, the ^{1}H-^{13}C-INEPT spectra of the *type-B** oligomers showed peak broadening only in PRE experiments performed when the paramagnetic center was located in the lipid head groups (Fig. S9); this suggests that dynamic regions of *type-B** oligomers do not insert in the hydrophobic interior of the lipid bilayer.

To characterize the structural nature of the regions of αS that are tightly bound to the lipid bilayers in the two types of oligomers, we measured ^{13}C-^{13}C-DARR spectra at -19 °C (Fig. 3D). This condition enhances the protein signals at the interface with this type of acidic lipid membrane (*24, 25*). In the case of the *type-A** oligomers, we observed an additional set of peaks whose resonances are characteristic of lysine residues, which are abundant in the region 1-97 of the αS sequence. The broad linewidths of these resonances, however, indicated the absence of a defined structural motif of *type-A** oligomers that is tightly bound to the membrane. In contrast, for the type-B* species we observed a set of additional resonances that closely matched those of the N-terminal 25 residues of monomeric αS bound to SUVs in an amphipathic α-helical conformation (*12, 25, 28*). Thus, the N-terminal region in the toxic oligomers is involved in promoting strong membrane interactions.

We next examined the effects that mutations in the N-terminal region of αS exert on the ability of *type-B** oligomers to disrupt biological membranes and induce cellular toxicity. The A30P αS variant (αS_{A30P}) is associated with an early onset form of PD and reduces the membrane affinity of the N-terminal region of αS (*24*). We also examined a truncated form of the protein lacking residues 2-9 ($\alpha S_{\Delta 2\text{-}9}$), a key region involved in anchoring the N-terminal region of αS to lipid membranes (*25, 29*). In vitro measurements of calcein release from POPS SUVs showed intermediate and negligible levels of membrane disruption by *type-B** oligomers formed from αS_{A30P} and $\alpha S_{\Delta 2\text{-}9}$, respectively, compared to the effects of wild type αS (αS_{WT}) *type-B** oligomers (Fig. S10A). Similar trends were observed in the disruption of cellular membranes by these species (Fig. S10B) and in their colocalization with the plasma membrane (Fig. S10D-E). The partial and a total impairment of the binding and disruption of cellular membranes by *type-B** oligomers of αS_{A30P} and $\alpha S_{\Delta 2\text{-}9}$, respectively, correlated highly with the levels of cellular toxicity generated by these species (MTT in Fig. S10C and ROS in Fig. S1B).

In conclusion, here we identified two structural elements that determine the ability of toxic αS oligomers to generate permeability of biological membranes (Figs. 3F, S11). In primary neurons and astrocytes this leads to an increase in the levels of basal intracellular Ca^{2+} and of ROS, and a consequent loss of cellular viability (*20, 21*). The first structural element is an exposed highly lipophilic region of the protein in the oligomers that promotes strong interactions with the membrane surface. The second is a rigid oligomeric core that is rich in β-sheet structure and is able to insert into the lipid bilayer and disrupt the membrane integrity. These conclusions are strongly supported by the introduction of specific mutations that partially (A30P) or completely (Δ2-9) suppress the membrane affinity of the N-terminal sequence of the protein. This suggests that the ability of the accessible N-terminal region of αS to bind strongly to lipid bilayers is a vital step in enabling oligomers to disrupt cellular membranes and consequently to induce neuronal toxicity.

References and Notes

1. F. Chiti, C. M. Dobson, Protein misfolding, amyloid formation, and human disease: A summary of progress over the last decade. *Annu Rev Biochem* **86**, 27-68 (2017).
2. V. N. Uversky, D. Eliezer, Biophysics of Parkinson's disease: structure and aggregation of alpha-synuclein. *Curr Protein Pept Sci* **10**, 483-499 (2009).
3. E. S. Luth, I. G. Stavrovskaya, T. Bartels, B. S. Kristal, D. J. Selkoe, Soluble, prefibrillar alpha-synuclein oligomers promote complex I-dependent, Ca^{2+}-induced mitochondrial dysfunction. *J Biol Chem* **289**, 21490-21507 (2014).
4. H. A. Lashuel, C. R. Overk, A. Oueslati, E. Masliah, The many faces of alpha-synuclein: from structure and toxicity to therapeutic target. *Nat Rev Neurosci* **14**, 38-48 (2013).
5. M. D. Tuttle *et al.*, Solid-state NMR structure of a pathogenic fibril of full-length human alpha-synuclein. *Nat Struct Mol Biol* **23**, 409-415 (2016).
6. M. Vilar *et al.*, The fold of alpha-synuclein fibrils. *Proc Natl Acad Sci U S A* **105**, 8637-8642 (2008).
7. J. A. Rodriguez *et al.*, Structure of the toxic core of alpha-synuclein from invisible crystals. *Nature* **525**, 486-490 (2015).
8. L. Bousset *et al.*, Structural and functional characterization of two alpha-synuclein strains. *Nat Commun* **4**, 2575 (2013).
9. G. Comellas, L. R. Lemkau, D. H. Zhou, J. M. George, C. M. Rienstra, Structural intermediates during alpha-synuclein fibrillogenesis on phospholipid vesicles. *J Am Chem Soc* **134**, 5090-5099 (2012).
10. B. Winner *et al.*, In vivo demonstration that alpha-synuclein oligomers are toxic. *Proc Natl Acad Sci U S A* **108**, 4194-4199 (2011).
11. M. Grey, S. Linse, H. Nilsson, P. Brundin, E. Sparr, Membrane interaction of alpha-synuclein in different aggregation states. *J Parkinsons Dis* **1**, 359-371 (2011).
12. N. Lorenzen, L. Lemminger, J. N. Pedersen, S. B. Nielsen, D. E. Otzen, The N-terminus of alpha-synuclein is essential for both monomeric and oligomeric interactions with membranes. *FEBS Lett* **588**, 497-502 (2014).
13. K. M. Danzer *et al.*, Different species of alpha-synuclein oligomers induce calcium influx and seeding. *J Neurosci* **27**, 9220-9232 (2007).
14. S. Campioni, et al, F. Chiti, A causative link between the structure of aberrant protein oligomers and their toxicity. *Nat Chem Biol* **6**, 140-147 (2010).
15. P. K. Auluck, G. Caraveo, S. Lindquist, alpha-Synuclein: membrane interactions and toxicity in Parkinson's disease. *Annu Rev Cell Dev Biol* **26**, 211-233 (2010).
16. J. H. Soper, V. Kehm, C. G. Burd, V. A. Bankaitis, V. M. Lee, Aggregation of alpha-synuclein in S. cerevisiae is associated with defects in endosomal trafficking and phospholipid biosynthesis. *J Mol Neurosci* **43**, 391-405 (2011).
17. S. W. Chen *et al.*, Structural characterization of toxic oligomers that are kinetically trapped during alpha-synuclein fibril formation. *Proc Natl Acad Sci U S A* **112**, E1994-2003 (2015).
18. D. E. Ehrnhoefer *et al.*, EGCG redirects amyloidogenic polypeptides into unstructured, off-pathway oligomers. *Nat Struct Mol Biol* **15**, 558-566 (2008).
19. N. Cremades *et al.*, Direct observation of the interconversion of normal and toxic forms of alpha-synuclein. *Cell* **149**, 1048-1059 (2012).
20. P. R. Angelova *et al.*, Ca2+ is a key factor in alpha-synuclein-induced neurotoxicity. *J Cell Sci* **129**, 1792-1801 (2016).

21. E. Deas *et al.*, Alpha-synuclein oligomers interact with metal ions to induce oxidative stress and neuronal death in Parkinson's disease. *Antioxid Redox Signal* **24**, 376-391 (2016).
22. M. J. Devine, et al, T. Kunath, Parkinson's disease induced pluripotent stem cells with triplication of the alpha-synuclein locus. *Nat Commun* **2**, 440 (2011).
23. G. Fusco *et al.*, Direct observation of the three regions in alpha-synuclein that determine its membrane-bound behaviour. *Nat Commun* **5**, 3827 (2014).
24. G. Fusco *et al.*, Structural basis of synaptic vesicle assembly promoted by alpha-synuclein. *Nat Commun* **7**, 12563 (2016).
25. G. Fusco *et al.*, Structural ensembles of membrane-bound alpha-synuclein reveal the molecular determinants of synaptic vesicle affinity. *Sci Rep* **6**, 27125 (2016).
26. P. Vallurupalli, G. Bouvignies, L. E. Kay, Studying "invisible" excited protein states in slow exchange with a major state conformation. *J Am Chem Soc* **134**, 8148-8161 (2012).
27. J. Milojevic, V. Esposito, R. Das, G. Melacini, Understanding the molecular basis for the inhibition of the Alzheimer's Abeta-peptide oligomerization by human serum albumin using saturation transfer difference and off-resonance relaxation NMR spectroscopy. *J Am Chem Soc* **129**, 4282-4290 (2007).
28. C. R. Bodner, C. M. Dobson, A. Bax, Multiple tight phospholipid-binding modes of alpha-synuclein revealed by solution NMR spectroscopy. *J Mol Biol* **390**, 775-790 (2009).
29. K. Vamvaca, M. J. Volles, P. T. Lansbury, Jr., The first N-terminal amino acids of alpha-synuclein are essential for alpha-helical structure formation in vitro and membrane binding in yeast. *J Mol Biol* **389**, 413-424 (2009).
30. F. A. Aprile *et al.*, Inhibition of alpha-Synuclein Fibril Elongation by Hsp70 Is Governed by a Kinetic Binding Competition between alpha-Synuclein Species. *Biochemistry* **56**, 1177-1180 (2017).
31. M. Johnson, A. T. Coulton, M. A. Geeves, D. P. Mulvihill, Targeted amino-terminal acetylation of recombinant proteins in E. coli. *PLoS One* **5**, e15801 (2010).
32. K. Wroblewski, R. Muhandiram, A. Chakrabartty, A. Bennick, The molecular interaction of human salivary histatins with polyphenolic compounds. *Eur J Biochem* **268**, 4384-4397 (2001).
33. K. Takegoshi, T. Terao, ^{13}C-^{1}H dipolar recoupling under very fast magic-angle spinning using virtual pulses. *Solid State Nucl Magn Reson* **13**, 203-212 (1999).
34. G. A. Morris, R. Freeman, enhancement of nuclear magnetic-resonance signals by polarization transfer. *J Am Chem Soc* **101**, 760-762 (1979).
35. H. Huang, J. Milojevic, G. Melacini, Analysis and optimization of saturation transfer difference NMR experiments designed to map early self-association events in amyloidogenic peptides. *J Phys Chem B* **112**, 5795-5802 (2008).
36. N. L. Fawzi, J. Ying, R. Ghirlando, D. A. Torchia, G. M. Clore, Atomic-resolution dynamics on the surface of amyloid-beta protofibrils probed by solution NMR. *Nature* **480**, 268-272 (2011).
37. E. L. Elson, D. Magde, Fluorescence correlation spectroscopy I. Conceptual basis and theory. *Biopolymers* **13**, 1-27 (1974).

38. S. Rajagopalan, F. Huang, A. R. Fersht, Single-molecule characterization of oligomerization kinetics and equilibria of the tumor suppressor p53. *Nucleic Acids Res* **39**, 2294-2303 (2011).

39. T. M. Laue, B. D. Shah, T. M. Ridgeway, S. M. Pellettier, Computer-aided interpretation of analytical sedimentation data for proteins. *Analytical Ultracentrifugation in Biochemistry and Polymer Science*, 90-125 (1992).

40. C. Capitini *et al.*, TDP-43 inclusion bodies formed in bacteria are structurally amorphous, non-amyloid and inherently toxic to neuroblastoma cells. *PLoS One* **9**, e86720 (2014).

41. R. Cascella *et al.*, Extracellular chaperones prevent Abeta42-induced toxicity in rat brains. *Biochim Biophys Acta* **1832**, 1217-1226 (2013).

42. E. Evangelisti *et al.*, Binding affinity of amyloid oligomers to cellular membranes is a generic indicator of cellular dysfunction in protein misfolding diseases. *Sci Rep* **6**, 32721 (2016).

43. G. Bongers *et al.*, The Akt/GSK-3beta axis as a new signaling pathway of the histamine H(3) receptor. *J Neurochem* **103**, 248-258 (2007).

44. M. Zampagni *et al.*, A comparison of the biochemical modifications caused by toxic and non-toxic protein oligomers in cells. *J Cell Mol Med* **15**, 2106-2116 (2011).

Acknowledgments. This research was supported by Parkinson's UK (G-1508 to G.F., M.V., C.M.D., A.D.), the UK Medical Research Council (MR/N000676/1 to G.F., M.V., C.M.D., A.D.), the Wellcome Trust (104933/Z/14/Z to A.D.), the Leverhulme Trust (RPG-2015-350 to A.D. and RPG-2015-345 to L.Y.), the British Heart Foundation (PG/14/93/31237 to A.D. and PG/11/81/29130 to L.Y.), the UK Biotechnology and Biological Sciences Research Council (BB/M023923/1 to A.D. and BB/G00594X/1 to L.Y.), the Agency of Science, Technology and Research of Singapore (to S.W.C.), the Ministry of Economy and Competitiveness of Spain (MINECO RYC-2012-12068 and MINECO/FEDER EU BFU2015-64119-P to N.C.), the Regione Toscana FAS-Salute (SUPREMAL to F.C., C.C., R.C), The Fondi di Ateneo of the University of Florence (to F.C, C.C.), and the Centre for Misfolding Diseases of the University of Cambridge.

The data supporting the findings of this study are available within the article and its Supplementary Materials.

Supplementary Materials
www.sciencemag.org
Materials and Methods
Figs. S1 to S12
Tables S1 to S2
References (*30-43*)

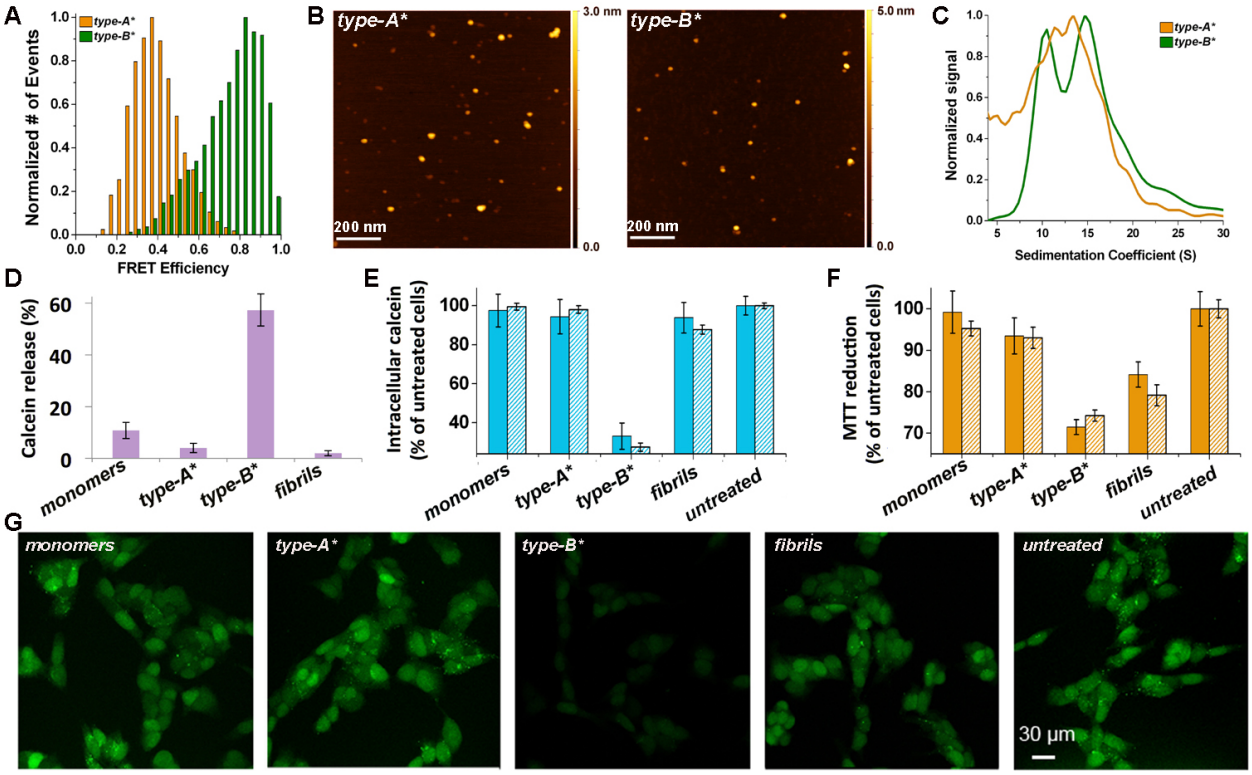

Figure 1. Properties of the two types of αS oligomers. (**A**) Intermolecular FRET efficiencies from measurements of *type-A** (orange) and *type-B** (green) αS oligomers. (**B**) Images of the *type-A** and *type-B** samples of αS oligomers probed by AFM (scale bar 200 nm). (**C**) Sedimentation coefficients of the *type-A** (orange) and the *type-B** (green) oligomers measured using AU. (**D**) In vitro calcein release (%) from POPS SUVs (see Methods). (**E-F**) Intracellular calcein-induced fluorescence (**E**) and mitochondrial activity monitored by the reduction of MTT (**F**) measured on human neuroblastoma SH-SY5Y cells (filled bars) and rat primary cortical neurons (striped bars) upon incubation with the various αS species. The data in panels D-F report the mean values ± standard deviations (see table S2 for P values). (**G**) Representative confocal scanning microscopy images of SH-SY5Y cells (scale bar 30 µm), showing intracellular calcein-induced fluorescence upon incubation with the various αS species.

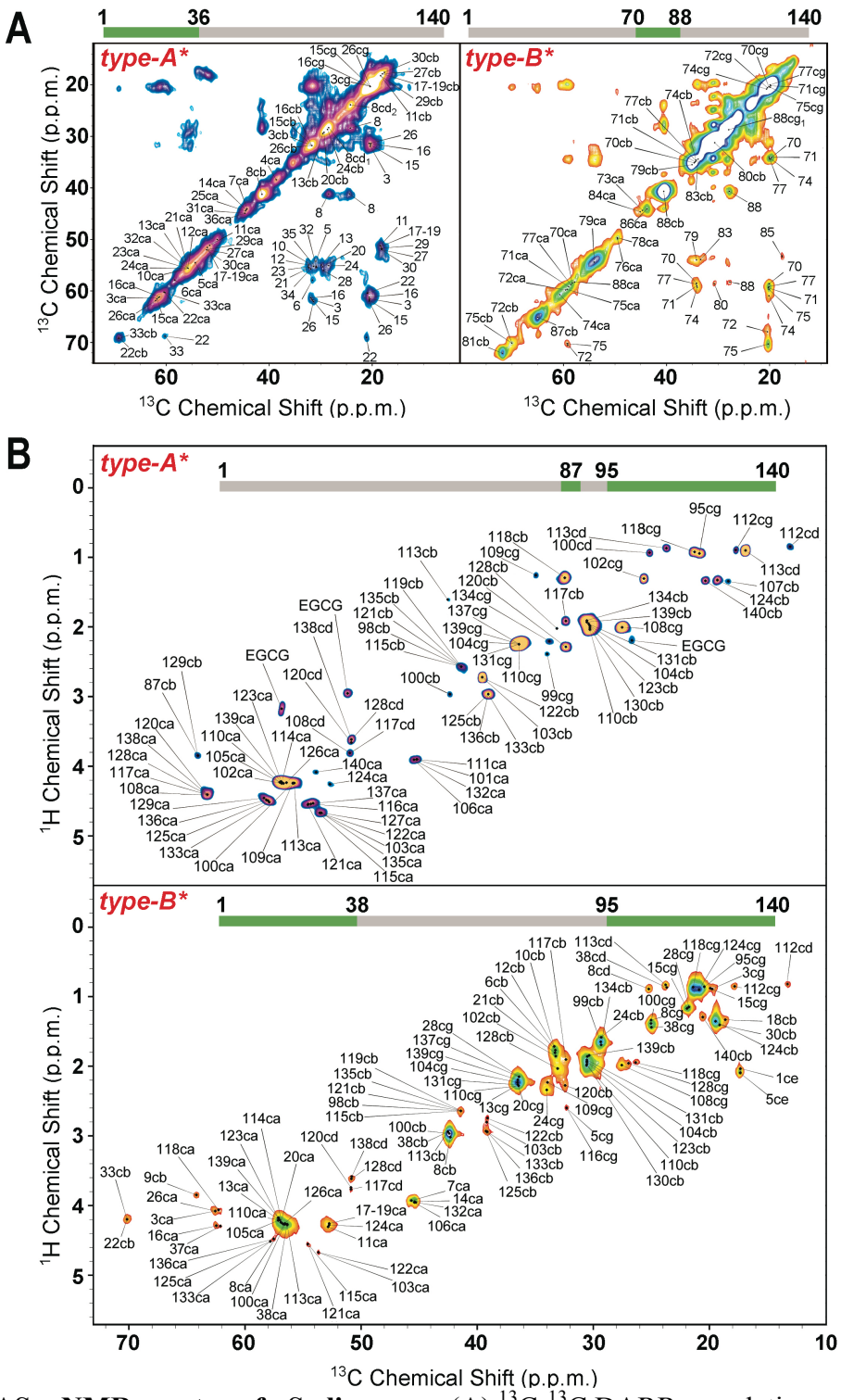

Figure 2. MAS ssNMR spectra of αS oligomers. (**A**) ^{13}C-^{13}C DARR correlation spectra (aliphatic regions) of *type-A** and *type-B** αS oligomers (left and right panels, respectively). (**B**) ^{1}H-^{13}C correlations via INEPT transfer. The labels ca, cb, cg, cd and ce indicate C^{α}, C^{β}, C^{γ}, C^{δ} and C^{ε} atoms, respectively. The regions of the protein sequence detected in the spectra are highlighted in green in the bars at the top of the spectra.

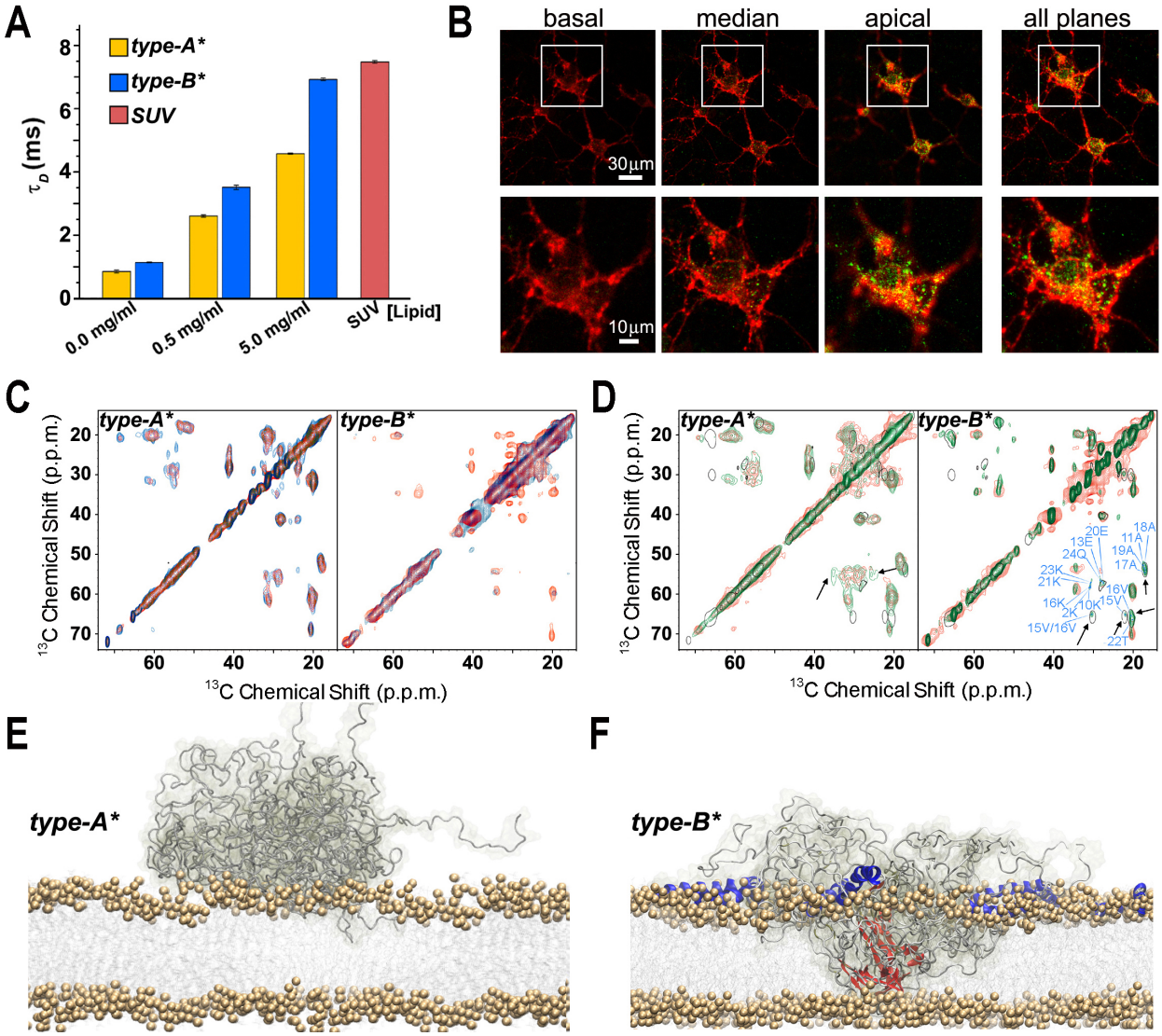

Figure 3. Interactions of αS oligomers with lipid bilayers. (**A**) Diffusion times, $\boldsymbol{\tau_D}$, from FCS experiments of *type-A** and *type-B** αS oligomers in the presence of variable quantities of SUVs composed of DOPE:DOPS:DOPC. $\boldsymbol{\tau_D}$ values and errors are derived from the fitting of the autocorrelation function (see Methods and Fig. S7). (**B**) Representative confocal scanning microscope images of basal, median, and apical planes and their combination (fourth column) of primary cortical neurons upon incubation of 15 min with *type-B** αS oligomers. Red and green fluorescence indicates the cell membrane and the αS oligomers, respectively. Lower panels correspond to magnifications of the sections indicated with a white square in the upper panels (**C**) PRE effects measured using MAS ssNMR for *type-A** (left) and *type-B** (right) αS oligomers using SUVs with a paramagnetic center at the position of carbon 16 of the lipid chain. ^{13}C-^{13}C-DARR spectra measured in the presence and absence of the paramagnetic labeled lipids are shown in blue and red, respectively. (**D**) ^{13}C-^{13}C-DARR spectra of isolated *type-A** (left) and *type-B** (right) αS oligomers (red) compared with spectra measured at -19 °C in the presence of DOPE:DOPS:DOPC SUVs (green) and of monomeric αS bound to the same type of vesicles (*24*) (black contour lines). The arrows identify the signals of residues in the αS oligomers arising from the membrane-bound protein regions. In the case of *type-B** αS oligomers these regions

were assigned from a previous study of the monomeric state of αS bound to SUVs (*24*). (**E-F**) Schematic representation of the binding of *type-A** and *type-B** with biological membranes. (**E**) *Type-A** (left) are mainly disordered and bind exclusively to the membrane surface. (**F**) *Type-B** αS oligomers feature both structured (red) and disordered (grey) regions, and bind the surfaces of the lipid bilayers *via* the N-terminal regions fold into amphipathic α-helices (blue) upon membrane binding. The rigid regions of *type-B** αS oligomers, which are rich in β-sheet structure, insert into the lipid bilayers thereby disrupting their integrity.